Monitoring Therapeutic Response to Anti-FAP CAR T Cells using [^{18}F]AlF-FAPI-74

Iris K. Lee[1,2], Estela Noguera-Ortega[3], Zebin Xiao[4], Leslie Todd[4], John Scholler[5], Decheng Song[5], Maria Liousia[3], Katheryn Lohith[2], Kexiang Xu[2], Kimberly J. Edwards[2], Michael D. Farwell[2], Carl H. June[5], Steven M. Albelda[3,5], Ellen Puré[4], Mark A. Sellmyer[2,6]*

1. Department of Bioengineering, University of Pennsylvania, Philadelphia, PA, USA. 2. Department of Radiology, Perelman School of Medicine, University of Pennsylvania, Philadelphia, PA ,USA. 3. Department of Medicine, Perelman School of Medicine, University of Pennsylvania, Philadelphia, PA USA. 4. Department of Biomedical Sciences, School of Veterinary Medicine, University of Pennsylvania, Philadelphia, PA, USA, 5. Center for Cellular Immunotherapies, Perelman School of Medicine, University of Pennsylvania, Philadelphia, PA, USA. 6. The Deparment of Biochemistry and Biophysics, Perelman School of Medicine, University of Pennsylvania, Philadelphia, PA, USA.

* Correspondence should be addressed to:
M.A.S. (mark.sellmyer@pennmedicine.upenn.edu)
https://orcid.org/0000-0002-1407-1905

Department of Radiology

Perelman School of Medicine at the University of Pennsylvania

813A Stellar-Chance Labs

422 Curie Boulevard

Philadelphia, PA 19104-6059

Phone: 215-573-3212

Running Title: Monitoring response to CAR T cell therapy using PET imaging

Keywords: Cellular therapy, FAP, biomarkers, molecular imaging, PET

Synopsis: A PET imaging approach targeting fibroblast activation protein (FAP) expressed on activated fibroblasts of the tumor stroma has the potential to predict and monitor therapeutic response to FAP-targeted CAR T cell therapy

Translational Relevance

Precision medicine is an emerging theme in modern cancer therapy, with the goal of tailoring treatments based on the presence or absence of certain biomarkers in the tumor. Approaches to targeted therapies have diversified, including genetically engineered cell therapies like chimeric antigen receptor (CAR) T cells. However, current tools to predict and monitor therapeutic responses to these dynamic, "living drugs" are limited. Here we show that a positron emission tomography (PET) radiotracer [^{18}F]AlF-FAPI-74 targeted to fibroblast activation protein (FAP), a pan-tumor marker expressed by activated fibroblasts in the tumor microenvironment, is able to image FAP expression in pre-clinical tumor models with high sensitivity. Coupled with FAP-targeted CAR T cells, [^{18}F]AlF-FAPI-74 PET imaging demonstrated successful clearance of FAP$^+$ cells following therapy, with a high correlation of PET signal to FAP signal quantified using immunohistochemistry. Our study highlights the potential role of [^{18}F]AlF-FAPI-74 as a predictive and pharmacodynamic imaging biomarker for FAP-targeted therapies in assessing the target biodistribution and informing patient selection, as well as in monitoring response to therapy.

Abstract

Purpose: Despite the success of chimeric antigen receptor (CAR) T cell therapy against hematological malignancies, successful targeting of solid tumors with CAR T cells has been limited by a lack of durable responses and reports of toxicities. Our understanding of the limited therapeutic efficacy in solid tumors could be improved with quantitative tools that allow characterization of CAR T-targeted antigens in tumors and accurate monitoring of response.

Design: We used a radiolabeled fibroblast activation protein (FAP) inhibitor (FAPI) [^{18}F]AlF-FAPI-74 probe to complement ongoing efforts to develop and optimize FAP CAR T cells. The selectivity of the radiotracer for FAP was characterized *in vitro* and its ability to monitor changes in FAP expression was evaluated using rodent models of lung cancer.

Results: [^{18}F]AlF-FAPI-74 showed selective retention in FAP$^+$ cells *in vitro*, with effective blocking of the uptake in presence of unlabeled FAPI. *In vivo*, [^{18}F]AlF-FAPI-74 was able to detect FAP expression on both tumor cells as well as FAP$^+$ stromal cells in the tumor microenvironment with a high target-to-background ratio. We further demonstrated the utility of the tracer to monitor changes in FAP expression following FAP CAR T cell therapy, and the PET imaging findings showed a robust correlation with *ex vivo* analyses.

Conclusion: This non-invasive imaging approach to interrogate the tumor microenvironment represents an innovative pairing of a diagnostic PET probe with solid tumor CAR T cell therapy and has the potential to serve as a predictive and pharmacodynamic response biomarker for FAP as well as other stromal cell-targeted therapies.

Introduction

Recent breakthroughs in chimeric antigen receptor (CAR) T cell therapy have positively transformed the management of many hematological malignancies (1). With such success, adoptive cell therapy is being explored for the treatment of solid tumors (2). The effort to extend the benefits of CAR T therapy to other cancers, however, is challenged by a lack of therapeutic efficacy and reports of severe toxicities. Robust biomarkers that can help identify patients likely to benefit from the therapy and accurately assess treatment response are needed to improve the safety of the therapy for patients. This problem is especially true in the context of CAR T cell treatment for solid tumors given the lack of uniformly expressed tumor-specific markers across different solid tumor types, which increases concern for on-target/off-tumor toxicities (3). Identification of biomarkers that can provide insights on the likelihood, as well as presence or absence of a therapeutic response, will help maximize the therapeutic potential of these "living drugs" and help inform patient management early in the treatment course.

The microenvironment surrounding tumor cells is a complex and dynamic system integral to solid tumor pathogenesis (4). Thus, the tumor microenvironment (TME) and supporting cells in the tumor stroma, which can be present across many different tumor types, make the TME a promising target to potentiate treatments like immunotherapies (5). Specifically, fibroblast activation protein (FAP), a cell surface serine protease that is highly expressed on cancer-associated fibroblasts (CAFs) in over 90% of epithelial cancers (6,7), has emerged as a pan-tumor target (8). Given increasing evidence that FAP and FAP^+ cells play a vital role in the remodeling of the tumor microenvironment and tumor progression, many FAP-targeted therapies – such as vaccines (9) and immunotherapies (10) – are in development. In concert with therapeutic developments targeting FAP, imaging probes which can quantitatively measure FAP expression have shown remarkable results. A recent retrospective analysis of patients imaged with Gallium-labeled FAP inhibitor ([^{68}Ga]-FAPI-04) showed significant tracer uptake in a variety of primary, metastatic, and recurring solid tumor entities (11), highlighting that such "universal" overexpression of FAP across different solid tumors not only make it a promising therapeutic target, but also a useful biomarker to assess for diagnosis and staging of different solid tumors.

Here, we investigate the use of [^{18}F]AlF-FAPI-74 PET pre-clinical imaging and its potential role in predicting and monitoring response to FAP CAR T cell therapy. FAP-targeted CAR T cells have demonstrated a significant anti-tumor effect in several pre-clinical solid tumor models including pancreatic cancers and mesothelioma (12-14). In this work, we characterize the *in vitro* and *in vivo* uptake of [^{18}F]AlF-FAPI-74 by FAP-expressing cells. We also demonstrate the utility of the tracer for monitoring therapeutic response following administration of a novel FAP (4G5) CAR T cell therapy in a pre-clinical lung carcinoma model that induces the formation of native mouse stroma. Using PET to help identify patients who are most likely to respond to the therapy based on the level of FAP expression in the tumor and monitor their response to the FAP-targeted CAR T cells could be key for clinical translation and integration of the therapy for patient management. Monitoring FAP expression over time could provide a direct way to assess the efficacy of FAP CAR T cell therapy by measuring how the target FAP-expressing cells are depleted in response, which is in contrast to traditional approaches that focus on tracking changes in tumor size during treatment, and could provide early insight into treatment success or failure.

Methods

Chemical Synthesis

The FAPI-74 precursor was synthesized by ABX advanced biochemical compounds gmbH (Radeberg, Germany). The manufacturing process of [^{18}F]AlF-FAPI-74 final drug product **(Figure 1A)** was adapted from

the manual process developed by Giesel *et al.* (15) and was carried out by SOFIE Biosciences, Inc. (Totowa, New Jersey, USA) on a Trasis miniAllinOne radiosynthesizer. Specific activity ranged from $2.43x10^4$-$9.37x10^4$ mCi/mg or 661.67-2550.14 GBq/µmol. Methods on chelator conjugation, radiolabeling, and quality control of the final, radiolabeled full-length 4G5 FAP antibody are described in the supplemental information under "DFO-Conjugation of Antibodies" and "Radiolabeling of Antibodies with Zirconium-89 (^{89}Zr)".

Cell Lines

Human mesothelioma cell line I45 wild type (WT) was originally derived from a sarcomatoid pleural mesothelioma and provided by Dr. Joseph Testa (Fox Chase Cancer Center, Philadelphia, PA). I45 cells were transduced with a lentivirus encoding human FAP and then flow-sorted to enrich for I45 huFAP cells. The human lung adenocarcinoma cell line A549 was purchased from the ATCC (ATCC CCL-185™). Cells were maintained in RPMI 1640 supplemented with 10% fetal bovine serum (FBS), 100 U/mL penicillin, and 100 µg/mL streptomycin sulfate, and cells were detached using Versene to prevent cleavage of FAP from the cell surface. All reagents were purchased from ThermoFisher Scientific.

***In Vitro* Cell Uptake Study**

$3x10^6$ I45 WT and I45 huFAP cells were incubated with $6x10^6$ counts per minute (cpm) (which corresponds to ~90-100µCi or ~3.3-3.7MBq) of [^{18}F]AlF-FAPI-74 for 60 minutes in the presence or absence of unlabeled 10µM FAPI-74 in media. Following incubation, cells were centrifuged at 1200 rpm and washed 3 times with cold PBS (21-031-CM, Corning). After the third wash, the cell pellet was resuspended in 600µL of PBS and split into 3 technical replicates of 200µL. Radiotracer uptake was quantified on a gamma counter (PerkinElmer) and analyzed by dividing counts by the counts of incubated dose of [^{18}F]AlF-FAPI-74 (injected dose; ID). The final uptake was reported as %ID normalized per 10^6 cells (%ID/10^6 cells). *In vitro* cell uptake studies with the full-length 4G5 antibody are described in the supplemental information under "*In Vitro* Cell Uptake Study with [^{89}Zr]DFO-4G5."

Generation of 4G5 Hybridoma

Full-length canine FAP cDNA was cloned by PCR from total RNA extract of canine osteosarcoma cells, SK KOSA. The PCR product was sequenced and cloned into pLenti/v5-D-TOPO which was used to generate virus and transduce Balb/C 3T3 cells. FAP-null mice were immunized and boosted four times intraperitoneally with the 3T3 cells expressing caFAP. Three days after the final boost, splenocytes were harvested and fused to myeloma cells. Hybridoma supernatants were screened by flow cytometry for mAbs that reacted specifically with MC KOSA.caFAP cells but not the parental MC KOSA cells which are negative for FAP. Clone 4G5 was further screened against MC KOSA canine osteosarcoma cells, mouse dermal fibroblasts, and human foreskin fibroblasts expressing canine, mouse, and human FAP, respectively, and showed species cross-reactivity **(Figure S1)**. ThermoFisher Rapid ELISA Mouse mAB Isotyping kit (#37503) was used to determine IgG1k isotype.

Generation of Anti-FAP CAR Construct

Total RNA isolated from 4G5 hybridoma cell line was reverse transcribed (Takara, Cat# RR057A) into cDNAs and PCR amplified using a library of mouse variable chain primers (Progen Cat# F2010) to identify hybridoma sequence. Additionally, 5' RACE was used to validate 5' most sequences (Invitrogen, Cat#18374058), these amplified bands were TOPO cloned and sequenced. The procedures were repeated to confirm the integrity of identified sequences. All isolated and sequence-verified ORFs of variable chains were synthesized and used in heavy and light chain combinations to obtain desired performing scFV in CAR format. For this study, a CAR construct containing the V_L and V_H sequences (L2HG) followed by CD8α hinge, CD8α transmembrane domain, and two human intracellular signaling domains (ICD) derived from

4-1BB and CD3ζ was synthesized and cloned into pTRPE lentiviral plasmid. This CAR targets both human and murine FAP-expressing cells. A T2A-mCherry gene was cloned downstream of the L2HG FAP CAR domain for assessment of transduction and flow-based sorting of CAR^+ T cells **(Figure 4A)**.

Generation of CAR T Cells

Primary human T cells collected from healthy volunteers were obtained from the Human Immunology Core at the University of Pennsylvania. All human specimens were collected under University Institutional Review Board-approved protocols following informed consent from the volunteers. Bulk T cells (containing both $CD4^+$ and $CD8^+$) were activated and expanded by incubating with anti-CD3/anti-CD28 antibody-coated magnetic beads (Dynabeads, Thermo Fisher Scientific) at a ratio of 3:1 beads to T cells. Following 16 hours of incubation with the beads, pTRPE FAP CAR-T2A-mCherry lentivirus (prepared as previously described (16)) was added to the T cells at an MOI of 5. The T cells were expanded for 10 days before characterization and cell sorting.

Flow Cytometry

FAP CAR-T2A-mCherry T cells were pelleted, resuspended in 2% BSA in PBS (Invitrogen), and incubated with Alexa Fluor® 647 AffiniPure F(ab'2) fragment goat anti-mouse IgG (Jackson ImmunoResearch Laboratories) for 30 minutes at room temperature. Stained cells were analyzed on an LSR II flow cytometer (BD Biosciences) for mCherry and CAR expression, and flow data were analyzed using FlowJo software.

Cytotoxicity and Cytokine Release Assay

$1x10^4$ of I45 WT and I45 huFAP target cells were seeded into 96-well plates. The following day, either non-transduced (NTD) – but activated – control T cells or effector FAP CAR-T2A-mCherry T cells were added to the target cells at a range of effector-to-target (E:T) ratios from 2.5:1 to 20:1. Following an overnight co-incubation of T cells and target cells, supernatants were collected to quantify IFNγ and TNFα release by ELISA (Abcam), and target cell viability was assessed using CellTiter 96® Aqueous Non-Radioactive Cell Proliferation Assay (MTS) (Promega).

I45 Mesothelioma Model

6- to 8-week-old female immunodeficient NOD-SCID-*Il2rg*$^{-/-}$ (NSG) mice were obtained from Penn Stem Cell & Xenograft Core and subcutaneously xenografted with $1x10^6$ I45 WT cancer cells on the left flank and $1x10^6$ I45 huFAP cancer cells on the right flank in 100µL of PBS. Following 2 weeks of tumor growth, when tumors reached ~100-150mm^3, animals were administered ~200-250µCi [^{18}F]AlF-FAPI-74 via tail vein and then anesthetized under 2% isoflurane for PET/CT imaging on a small animal PET/CT (Molecubes) 1 hour post-radiotracer administration. For image analysis, 3-dimensional (3D) elliptical regions of interest (ROIs) were drawn around the tumor and muscle (background organ) using the CT images as a reference, and the ROIs were copied to PET. The maximum and mean counts from each ROI were quantified using MIM (MIM Software). The ratio of tracer uptake between tumor and muscle (tumor-to-muscle ratio) was calculated by dividing SUV_{max} of tumor by SUV_{max} of muscle, or dividing SUV_{mean} of tumor by SUV_{mean} of muscle. PET image scale bar is represented in unit of Scaled Threshold of $SUV_{body\ weight}$ (SUV_{bw}) and CT image scale bar is Houndsfield Unit (HU). PET studies with [^{89}Zr]DFO-4G5 are described in the supplemental information under "[^{89}Zr]DFO-4G5 Small Animal PET Imaging".

A549 Lung Adenocarcinoma Model

6- to 8-week-old female immunodeficient NSG mice were subcutaneously xenografted with $1x10^6$ A549 cancer cells on the right flank in 100µL of PBS. Following 3 weeks of tumor growth, when the tumors reached ~100-150mm^3, [^{18}F]AlF-FAPI-74 PET/CT imaging was performed and analyzed as described above. For the clearance experiment with FAP CAR T cells, all mice were injected intravenously (i.v.) with either

$5x10^6$ CAR^+ FAP CAR-T2A-mCherry T cells or non-transduced (NTD) control T cells the day after baseline [^{18}F]AlF-FAPI-74 PET/CT imaging was performed. A follow-up scan was performed 14 days post-T cell injection.

***Ex Vivo* Biodistribution and Tissue Analysis**

Mice were sacrificed following terminal [^{18}F]AlF-FAPI-74 PET/CT imaging. Various tissues were harvested for *ex vivo* biodistribution analysis and the level of uptake in each organ was measured using a gamma counter (PerkinElmer) and quantified as %ID per gram of organ (%ID/g). Tumor tissues were digested in a solution of BD Horizon™ Dri Tumor & Tissue Dissociation Reagent (BD Biosciences) for 30 minutes at 37°C. Digested tumors were filtered through 70µm nylon mesh cell strainers (Fisher Scientific), and red blood cells were lysed as needed (Pharm Lyse, BD Biosciences). Single-cell suspensions (1×10^6 cells) were stained with PE-Dazzle 594-conjugated anti-human CD45 antibody (344744, Biolegend). *Ex vivo* biodistribution analysis of [^{89}Zr]DFO-4G5 is described in the supplemental information under "E*x Vivo* Biodistribution Analysis of "[^{89}Zr]DFO-4G5 in Healthy (Non-Tumor Bearing) Animals".

Immunohistochemistry

Samples were frozen in OCT-embedding media on dry ice. 5µm sections were generated using a Cryostat (Leica CM 1950), mounted on glass slides (12-550-15, Fisher Scientific), and dried. Sections were washed with PBS for 5 minutes, incubated with blocking buffer containing 3% BSA (BSA-50, Rocklandand) and 0.3% Triton X-100 (10789704001, Roche) in PBS (21-031-CM, Corning) for 1 hour, and then stained with primary antibodies in blocking buffer overnight at 4°C. The following primary antibodies were used: rabbit monoclonal anti-fibroblast activation protein alpha (FAP-α; ab207178, Abcam), goat polyclonal anti-platelet-derived growth factor receptor alpha (PDGFRα; AF1062, R&D system), and FITC-conjugated mouse anti-mouse/human α-smooth muscle actin (F3777, Millipore Sigma). Following staining with primary antibodies, slides were blocked again for 1 hour and then incubated with secondary antibodies in the blocking buffer for 1 hour. All secondary antibodies (Alexa 555 Donkey anti-rabbit IgG (A32794) and DyLight 650 Donkey anti-goat IgG (84545)) were purchased from Invitrogen. Slides were washed 3 times and mounted in ProLong™ Diamond Antifade Mountant with DAPI (P36971, ThermoFisher). Low-magnification and high-magnification photos were taken using a Nikon NIS-Elements microscope and all images were processed using ImageJ.

Statistical Analyses

All the statistical data analysis was performed on Prism 9 (GraphPad). An unpaired, two-tailed student t-test was used to determine statistical significance between two groups. For comparisons of more than two groups, one-way or two-way ANOVA was performed with appropriate *post hoc* testing. A p-value of <0.05 was considered to be statistically significant. All data points are presented as mean $\pm$ SD.

Results

An ImmunoPET approach demonstrates limited dynamic range in detecting FAP *in vivo*

To identify the *in vivo* antigen target of FAP-directed CAR T cells, and thereby serve as a predictive biomarker of FAP CAR T cell therapy, one approach would be to use an immunoPET agent. In this approach, the antibody-derived radiotracer shares the identical clonal origin and the single-chain variable fragment (scFv) that will bind the same epitopes as the FAP CAR T cells. The Puré lab developed a mouse IgG1k monoclonal antibody, 4G5, against canine FAP that cross-reacts with human and mouse FAP **(Figure S1)**. A CAR was engineered based on the 4G5 monoclonal antibody and cloned into a lentiviral vector encoding 4G5 anti-FAP scFv (4G5)-CD8 hinge-4-1BB-CD3z. In order to test whether we can detect FAP expression using the 4G5 antibody that is parent to the FAP CAR T cell therapy in development, we

radiolabeled the full-length 4G5 FAP antibody with ^{89}Zr to develop a [^{89}Zr]DFO-4G5 immunoPET probe. Successful conjugation of 4G5 to chelator deferoxamine (DFO) – with a degree of labeling (DOL) of 2.6 DFO molecules per antibody – was confirmed by MALDI-TOF (**Figure S3A**). The radiochemical yield of ^{89}Zr radiolabeling ranged from 70-82% with a specific activity of 6.5-9.3mCi/mg and the free ^{89}Zr in the final product, as assessed by radio TLC, was minimal (**Figure S3B**). Methods of DFO-conjugation, radiolabeling of the antibody, and subsequent downstream assays performed with [^{89}Zr]DFO-4G5 are described in the supplemental information. To evaluate the ability of [^{89}Zr]DFO-4G5 to selectively bind to FAP, an *in vitro* cell uptake experiment was performed with: I45 WT (which do not express FAP) and I45 cells transduced to express human FAP (I45 huFAP) **(Figure S2)**. The uptake study showed a 54-fold higher tracer uptake in I45 huFAP cells compared to I45 WT, demonstrating a high specificity of the [^{89}Zr]DFO-4G5 immunoPET probe for FAP **(Figure S3C).** Co-incubation of the radiotracer with excess unlabeled 4G5 antibody successfully competed with and reduced the uptake of the radiotracer by I45 huFAP, further demonstrating the specificity of the radiotracer uptake via FAP binding.

Given the high specificity demonstrated in the uptake study, the [^{89}Zr]DFO-4G5 radiotracer was next tested for its ability to detect FAP expression in two different tumor xenograft models: 1) I45 mesothelioma (non-stromagenic) and 2) A549 lung adenocarcinoma model where the tumor cells do not express FAP but drive the generation of FAP$^+$ stromal cells in the tumor microenvironment *in vivo* (13). For the I45 model, the I45 WT and I45 huFAP tumor cells were xenografted on opposite flanks of immunodeficient NSG mice. Following 2 weeks of tumor growth, [^{89}Zr]DFO-4G5 radiotracer was administered via tail vein and PET/CT images were acquired 72 hours post-radiotracer administration. In this I45 model, [^{89}Zr]DFO-4G5 PET/CT uptake was 3-fold higher in the I45 huFAP tumor compared to the I45 WT **(Figure S3D)**. *Ex vivo* anti-FAP IHC and autoradiography on tumor sections further supported the imaging findings **(Figure S4B)**. For the A549 model, the cells were also xenografted on the flank of NSG mice and grown for 3 weeks. The A549 tumor showed approximately 8 to 9-fold increased radiotracer uptake relative to the muscle **(Figure S3E)**, and this was further supported in the ex vivo biodistribution analysis **(Figure S4A, right panel)**.

Despite the promising data showing a robust accumulation of the tracer in FAP-expressing tumors, a few limitations of this approach became apparent in the validation process. Both PET imaging and *ex vivo* biodistribution analysis showed evidence of tracer uptake in non-target expressing I45 WT tumor that was around 5-fold higher than the background, which demonstrates potential non-specific accumulation of antibody-based probe in areas of leaky tumor vasculature **(Figure S3D and Figure S4A, left panel)**. Lastly, as a full-length IgG radiotracer, [^{89}Zr]DFO-4G5 exhibited slow accumulation and clearance kinetics **(Figure S4C)**, and PET imaging had to be performed 3 days following tracer injection to ensure optimal target-to-background ratio. While this was feasible to accommodate for pre-clinical imaging studies, same-day imaging would be ideal for a future clinical workflow. As small molecule-based imaging probes are rapidly cleared from blood due to their relatively small size and will thereby help improve the target-to-background ratios, we next evaluated the use of a known radiolabeled small molecule inhibitor of FAP (FAPI), [^{18}F]AlF-FAPI-74, as an alternative PET radiotracer to monitor FAP expression and thereby complement FAP-targeted therapies.

Small molecule-based [^{18}F]AlF-FAPI-74 radiotracer exhibits high specificity for FAP

The specificity of [^{18}F]AlF-FAPI-74 tracer **(Figure 1A)** for FAP was tested by performing an *in vitro* cell uptake experiment with I45 cells. The uptake study showed significantly higher tracer uptake of over 100-fold in the I45 huFAP cells compared to the I45 WT. This uptake was effectively competed by the addition of an excess of unlabeled FAPI, demonstrating rapid and highly specific binding of [^{18}F]AlF-FAPI-74 tracer to FAP *in vitro* **(Figure 1B).**

[^{18}F]AlF-FAPI-74 imaging of FAP in xenograft tumor models demonstrates enhanced sensitivity and dynamic range

To evaluate the ability of the [^{18}F]AlF-FAPI-74 radiotracer to detect FAP expression in animals, we tested the FAPI tracer in both the I45 mesothelioma and A549 lung adenocarcinoma model used for the initial validation of the [^{89}Zr]DFO-4G5 radiotracer. In the I45 model, [^{18}F]AlF-FAPI-74 uptake was higher by 7.5-fold in the I45 huFAP tumor compared to the I45 WT **(Figure 2A and 2B)**. This degree of uptake was more than 2-fold higher than what was observed with [^{89}Zr]DFO-4G5 **(Figure S3D)**. *Ex vivo* biodistribution analysis further supported and validated the PET imaging findings, with 12 and 15-fold increased tracer retention in the I45 huFAP tumor relative to the I45 WT tumor and background organs, respectively **(Figure 2C)**. To validate that the increased PET signal in the I45 huFAP tumor was in fact due to its FAP expression, we performed anti-FAP IHC and showed selective expression of FAP in the I45 huFAP tumor **(Figure 2D)**. Probing for α-smooth muscle actin-positive (αSMA$^+$) myofibroblasts and platelet-derived growth factor receptor α-positive (PDGFRα$^+$) cells (which represent subpopulations of the heterogenous CAFs found in the tumor microenvironment (17)), we did not detect significant numbers of CAFs in the non-stromagenic I45 WT or I45 huFAP tumors as expected, indicating that the PET signal is mainly attributable to uptake by the I45 cells engineered to express FAP.

In the A549 model, animals xenografted with the tumor showed approximately 4 to 6-fold increased [^{18}F]AlF-FAPI-74 uptake in the A549 tumor relative to the muscle **(Figure 3A and 3B).** As A549 cells do not express FAP, the PET signal in this model is attributable to FAP$^+$ stromal cells in the tumor microenvironment. We were able to clearly identify fibroblasts in this stromagenic tumor with IHC **(Figure 3C)**. IHC images of the A549 showed a variable pattern of FAP expression related to fibroblast invasion and recruitment to the stroma, compared to the I45 model which exhibited a more homogenous population of FAP$^+$ cells given its expression by the tumor cells themselves. An imaging study with FAP knockout (KO) NSG mice bearing A549 tumors showed an absence of tracer uptake in the area of the tumor **(Figure S5)**, demonstrating that our [^{18}F]AlF-FAPI-74 tracer is specific for FAP and detects host stromal cells.

[^{18}F]AlF-FAPI-74 PET/CT imaging has utility in monitoring therapeutic response following FAP CAR T cell therapy

Given that [^{18}F]AlF-FAPI-74 can provide semi-quantitative index of FAP expression in the tumor microenvironment– the target of FAP-directed therapies – it has the potential to not only serve as a predictive biomarker that can be used to stratify patients who are likely to respond to therapy but also as a downstream measure of therapeutic efficacy (i.e. how effective FAP-targeted therapies are at ablating the target FAP$^+$ cells). In order to test this premise, we evaluated whether [^{18}F]AlF-FAPI-74 tracer can detect clearance of FAP$^+$ cells in the more challenging, biologically relevant A549 tumor model following FAP CAR T cell treatment.

For these studies, we utilized a new FAP CAR construct based on the scFv of the 4G5 antibody which also expressed mCherry as a marker gene (**Figure 4A).** We first demonstrated good expression levels of both the CAR and mCherry in transduced human T cells **(Figure 4B)**. We next confirmed their antigen-dependent ability to effectively kill I45 huFAP cells and spare non-FAP expressing I45 WT cells in an *in vitro* cytotoxicity study **(Figure 4C)**. Supernatants collected from the killing assay confirmed the release of IFNγ when the effector cells were co-incubated with FAP$^+$ target cells, indicating FAP-specific CAR T cell activation **(Figure 4D).**

NSG mice bearing 100-150mm^3 A549 tumors were injected with either 5x10^6 FAP CAR$^+$ T cells or non-transduced (NTD) control T cells following a baseline [^{18}F]AlF-FAPI-74 scan. Tumor volumes were measured every 3-4 days, and a follow-up scan was performed on Day 14 post-T cell injection **(Figure 5A)**. At this 14-day time point, mice treated with FAP CAR T cells had significantly smaller tumors ($p<0.01$) relative to the NTD control T cell-treated group, highlighting the therapeutic efficacy of the FAP CAR T cell therapy **(Figure 5B)**.

In the follow-up [^{18}F]AlF-FAPI-74 scan, there was no detectable tracer uptake in the area of tumor in mice that received FAP CAR T cell therapy while the NTD control T cell-treated group had a significant accumulation of tracer in the tumor region **(Figure 5C)**. Quantification of PET images showed that the tumor-to-muscle ratio decreased for FAP CAR T cell-treated group by 2 to 3-fold relative to the baseline scan, highlighting that the [^{18}F]AlF-FAPI-74 is a sensitive tool that allows imaging of FAP clearance from the tumor following a FAP-targeted therapy **(Figure 5D)**. Furthermore, we observed a robust correlation between the caliper measurements and tumor volume assessed by CT **(Figure S6)**.

To further validate the PET imaging findings, *ex vivo* analyses were performed after the terminal follow-up [^{18}F]AlF-FAPI-74 PET/CT scan. We observed a marked 3.5-fold higher retention of the tracer in the harvested tumors treated with NTD T cells relative to the FAP CAR T cell-treated tumors **(Figure 6A)**. While uptake in normal background tissues (blood, eye, spleen, muscle) was very low and comparable across the control and FAP CAR-treated groups, there was a statistically significant difference in bone and marrow uptake between the two groups. Flow analysis of cell population in the A549 tumor showed a higher percentage of total CD45$^+$ T cells in the CAR T-treated group relative to the NTD T cell-treated group, which indicated specific CAR T cell infiltration in the tumors **(Figure 6B)**. To further validate PET imaging findings, we again performed correlative anti-FAP, anti-αSMA, and anti-PDGFRα$^+$ IHC on the FAP CAR T-treated and NTD T cell-treated A549 tumors. Treatment with FAP CAR T cells abolished all subpopulations of CAFs, supporting that the lack of PET imaging signal in the tumor area is due to the successful depletion of FAP$^+$ cells **(Figure 6C)**. Disruption of all of the CAFs is expected in the FAP CAR T cell-treated group given that FAP$^+$ cells often co-express SMA and PDGFRα (17). Moreover, FAP$^+$ cells have shown to be critical to the recruitment and/or differentiation of SMA$^+$ myofibroblasts, and therefore depletion of FAP$^+$ cells will also disrupt the network of SMA$^+$ myofibroblasts as demonstrated in the IHC (13).

Discussion

The ability to monitor the biological target of a living drug such as CAR T cells is an important strategy where molecular imaging can support improvement and development of next-generation therapies (18). Here, we found that the inherent characteristics of small molecule-based radiotracers, such as the rapid clearance from background organs, allowed for high contrast imaging, and have advantages to characterize FAP expression compared to antibody-based immunoPET that requires conjugation to longer-lived isotopes. We demonstrated that [^{18}F]AlF-FAPI-74 extends beyond its role as a companion diagnostic (in predicting response) and can also serve as a “pharmacodynamic” biomarker to assess the downstream efficacy of a therapy. Thus, this approach has the potential to aid in both patient selection and in monitoring response to FAP-targeted therapies, including living drugs such as FAP CAR T cells as demonstrated here. Although similar tools, namely [^{89}Zr]-Atezolizumab (19) and [^{18}F]-FluorThanatrace (20), have been developed to help predict patient benefit from cancer therapies such as PD-1/PD-L1 checkpoint blockade therapy and PARP inhibitors, respectively, this work builds on these prior studies and demonstrate how a companion diagnostic tool can also be applied for a living drug where therapeutic production costs are significant. FAP-specific antibody-drug conjugates (ADCs) (21), tumor vaccines

against FAP (9), and radionuclide therapy with [^{177}Lu]FAPI-46 (22) are other FAP-targeting strategies that will use and benefit from [^{18}F]AlF-FAPI-74 imaging in a theranostic approach.

FAP-targeted nuclear imaging has been previously attempted with FAP antibodies (23,24) and boronic acid-based FAP inhibitors (25). However, given the extended half-life of these agents in the blood and poor target-to-blood ratio, quinoline-based small molecule FAPI tracers that offer high specificity and rapid blood clearance have ascended (26). Furthermore, FAPI tracers have already demonstrated potential as a diagnostic tool in different clinical settings beyond oncology, including in cardiovascular and autoimmune-mediated diseases (11,27-29). Our choice of the [^{18}F]AlF-FAPI-74 was informed by the extensive work of the Heidelberg group and medicinal chemistry optimization of FAPI compounds, several of which are near clinical translation (15). Similar to the observations in the field, while our 4G5 antibody-based immunoPET approach allowed us to visualize the antigenic target of FAP-directed CAR T cells given the shared scFv domains between the companion diagnostic and the therapeutic, the slow accumulation and clearance kinetics of the full-length antibody did not provide as high of sensitivity compared to the small molecule FAPI approach **(Figure S3D-S3E)**. Given that the tracer and the therapeutic share the same scFv domain, there is also a potential concern that the long half-life of the tracer may competitively inhibit CAR T antigen on the tumor and prevent the CAR T cells from eliciting cytotoxic effects. Moreover, the need for conjugation with radionuclides with extended half-lives and a long period between radiotracer administration and imaging is not conducive to clinical translation. Our decision to use ^{18}F-radiolabeled FAPI was a strategic choice to address this issue as ^{18}F is a scaleable radioisotope used in routine clinical PET imaging (e.g. [^{18}F]FDG imaging in oncology) (30) and would facilitate transition into the clinic in terms of both productions and meeting the clinical demand.

One of the key challenges of FAP-targeted therapies is that the antigen is also expressed at low levels in limited healthy tissues including bone marrow mesenchymal stem cells, muscle, and the pancreas (31,32). From the *ex vivo* biodistribution analysis following [^{18}F]AlF-FAPI-74 imaging, we were able to identify organs that have endogenous FAP expression in our xenograft mouse model and the potential effect of FAP CAR T cell therapy on these organs **(Figure 6A)**. For example, the %ID/g in both the bone marrow and the bone of the FAP CAR T cell-treated group was reduced compared to the NTD T cell-treated group. This suggests that there is some FAP expression in both the bone marrow and the bone of NSG mice, and the cells expressing FAP in these organs are affected by FAP CAR T cell therapy. Bone marrow suppression is a reported outcome of FAP CAR T cell therapy in different mouse models (32,33), however, immunohistochemical staining and flow cytometry studies showed differences in FAP expression in mouse versus human bone marrow (unpublished). Furthermore, a human biodistribution study with [^{18}F]AlF-FAPI-74 demonstrated low uptake in normal organs (15), providing support that FAP expression is limited in healthy adult tissues. Regardless, the overall finding highlights the potential clinical utility of [^{18}F]AlF-FAPI-74 in identifying patients who are likely to have an on-target/off-tumor toxicity in case of increased FAP expression at an off-tumor site, for example in the case of a healing wound or unknown fibrotic process. In addition to its potential use in the clinic, the tool may also be applied in pre-clinical settings to aid in the development of CAR T cell clinical protocols, including in the assessment of scFv affinity and different armoring strategies, to maximize the therapeutic window and minimize on-target/off-tumor toxicity. In our model, other organs of concern such as the pancreas and muscle did not have significant FAP expression that was affected by FAP CAR T cell therapy.

In this study, we demonstrated a clear correlation between [^{18}F]AlF-FAPI-74 imaging and IHC of the FAP^{+} tumors. For example, our PET imaging was able to pick out the uniform, homogenous expression of FAP in the I45 huFAP tumor **(Supplemental Video S1)** whereas the A549 tumor showed heterogeneous and patchy foci of tracer uptake from the infiltrating fibroblasts **(Supplemental Video S2)**. Such differential

pattern of uptake between the two tumors was also apparent in *ex vivo* IHC **(Figure 2D and Figure 3C)**. Correlating the [^{18}F]AlF-FAPI-74 PET signal and FAP signal quantified by IHC following treatment with either FAP CAR T cells or NTD control T cells, we observed a strong, positive relationship between the two measurements **(Figure S7)**. This highlights the potential of [^{18}F]AlF-FAPI-74 imaging to complement biopsy-based IHC as well as map out and monitor target expression following a therapeutic intervention. While the tumor sizes were still measurable following CAR T cell therapy, they were smaller compared to the non-transduced T cell-treated group **(Figure 5B)** and could have introduced a small, but possible quantification bias (partial volume effect). In the future, using reconstruction parameters that can help increase the effective resolution or applying appropriate correction methods could help minimize the bias (34,35).

While our data support that [^{18}F]AlF-FAPI-74 PET is an ideal candidate for non-invasive characterization of FAP expression and for monitoring of response to FAP CAR T cell therapy, future studies should focus on evaluating whether the observed changes in FAP expression ultimately predict long-term therapeutic success in terms of progression-free and overall survival and whether the degree of tracer uptake corresponds to and is a strong predictor of response to FAP CAR T cell therapy. This would be important given that FAP$^+$ cells tend to regenerate over time following therapy (13), and long-term monitoring of patients with [^{18}F]AlF-FAPI-74 PET would help inform clinical decision-making (e.g. re-dosing or dose optimization, change of therapy, etc.).

FAP CAR T cell therapy has the potential to be used in conjunction with other immunotherapies and potentiate their use in the clinic given its unique ability to permeabilize dense tumor microenvironment and tear down the physical barrier masking the tumor antigens (10). Therefore, imaging probes that can untangle the efficacy of one therapy from another will be useful in guiding patient care. For example, FAP CAR T cells have been paired with PD-1 blocking antibody and showed that the combination therapy results in better tumor control and improved survival in a humanized model of malignant pleural mesothelioma (36), a clinical indication where PD-1 blockade had previously failed to demonstrate a strong therapeutic response (37). In such dual-therapy models, monitoring and re-assessing FAP expression with a tool like [^{18}F]AlF-FAPI-74 PET may be critical in understanding whether the therapy is working as expected and also in identifying the ideal time to initiate the second therapy. PET imaging approaches can help to separate the results from complex therapies and can offer complementary data to the standard of care approaches such as IHC and serum biomarkers.

Although FAP is generally expressed at low levels in healthy tissues, its upregulation has been implicated in a wide range of non-oncologic indications (38). For example, FAP-targeted CAR T cells have been shown to specifically target activated cardiac fibroblasts and significantly reduce cardiac fibrosis to restore cardiac function (39). Pulmonary fibrosis is another fibrotic condition characterized by high FAP expression, and could also benefit from non-invasive characterization of FAP expression (40). Currently, there are very few drugs approved for the treatment of fibrotic conditions (41). Although the development of such drugs to treat fibrosis is a high priority, one potential limitation will be the ability to distinguish “active fibrosis” from “scar”. The former will likely be much more amenable to therapies such as kinase inhibitors, drugs targeted to fibroblasts, or cytokine and growth factor inhibitors. Since FAP is primarily expressed during active tissue remodeling (42), the ability to use FAPI imaging to both screen for the most potentially treatable patients and then to follow the response to treatments could be paradigm-changing. Furthermore, cardiotoxicity is a known complication of many cancer treatments, including immunotherapies such as checkpoint inhibitors (43). Detection of activated cardiac fibroblasts using FAPI imaging could help understand signs of immunotherapy-induced myocardial damage early in the treatment course, prevent further cardiotoxicity, and guide clinical care (44,45). The molecular

imaging biomarker paradigm presented in this work aims to provide a better understanding of target biology and heterogeneity, and thereby help tailor therapies to deliver personalized precision medicine to patients.

Disclosure of Potential Conflicts of Interest

SMA and EP report receiving research support for pre-clinical studies of FAP CAR T cells in solid tumors from TMUNITY and both are co-founder of CAPSTAN Therapeutics Inc. and receive research funding from the company for pre-clinical studies of FAP CAR T cells in fibrosis. CHJ: Royalties from Novartis. Scientific advisor for AC Immune, Alaunos, BluesphereBio, Cabaletta, Capstan, Carisma, Cartography, Cellares, Celldex, DeCART, Decheng, Poseida, Verismo, Viracta, and WIRB-Copernicus Group. MAS is a co-founder of Vellum Biosciences related to PET imaging of genetic therapies. The other authors declare no potential conflicts of interest.

Author Contributions

Conception and design: I. Lee, S. Albelda, E. Puré, M. Sellmyer

Development of reagents and methodology: I. Lee, E. Noguera-Ortega, Z. Xiao, L. Todd, K. Lohith, D. Song, J. Scholler, C. June

Acquisition of data (provided animals, acquired and managed patients, provided facilities, etc.): I. Lee, E. Noguera-Ortega, Z. Xiao, L. Todd, K. Lohith, M. Farwell, S. Albelda, E. Puré, M. Sellmyer

Analysis and interpretation of data (e.g., statistical analysis, biostatistics, computational analysis): I. Lee, E. Noguera-Ortega, Z. Xiao

Writing, review, and/or revision of the manuscript: I. Lee wrote the draft of the manuscript, with all authors, especially E. Noguera-Ortega, Z. Xiao, S. Albelda, E. Puré, and M. Sellmyer contributing to the revision.

Administrative, technical, or material support (i.e., reporting or organizing data, constructing databases): M. Sellmyer

Study supervision: M. Sellmyer

Acknowledgments

We thank members of the UPenn Human Immunology Core, the Small Animal Imaging Facility (Eric Blankemeyer), and the Flow Cytometry and Cell Sorting Facility. We thank Sherly Mosessian, Frank Valla (SOFIE Biosciences), and David Barrett (Tmunity) for their comments. Illustrations were created with Biorender.com. MAS is supported by the National Institute of Health Office of the Director Early Independence Award (DP5-OD26386), Burroughs Wellcome Fund Career Award for Medical Scientists. IKL and this research was supported by Institute for Translational Medicine and Therapeutics (ITMAT). SMA and EP are supported by P01 CA217805 from the National Cancer Institute. We also would like to acknowledge the Kathleen M. Rotz Lung Cancer Research Fund for partial support of this study.

Figures

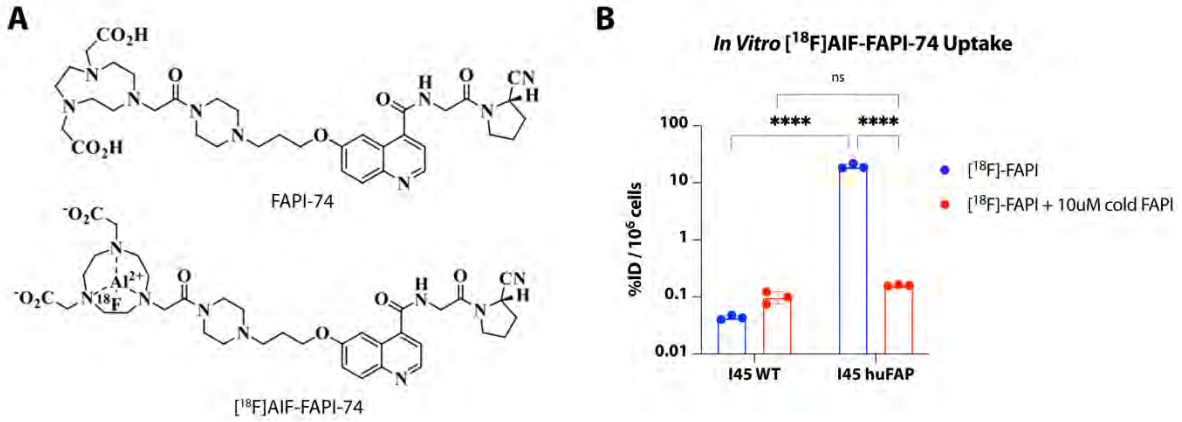

Figure 1. Structure of [^{18}F]AlF-FAPI-74 and its uptake in FAP-expressing cells *in vitro.*
(A) Structure of FAPI-74 and radiolabeled [^{18}F]AlF-FAPI-74. **(B)** 1x10^{6} I45 WT and human FAP-transduced I45 cells (I45 huFAP) were incubated with [^{18}F]AlF-FAPI-74 for 1 hour at 37°C in the presence or absence of unlabeled FAPI (10µM). The *in vitro* uptake study demonstrated a greater than 100-fold increased uptake of the tracer in I45 huFAP cells relative to WT and blocked controls. n=3, data points are mean ± SD. Uptake was measured as percent injected dose per gram (%ID/g) with a gamma counter. Groups were compared using a two-way ANOVA with Tukey's multiple comparisons test. ****p<0.0001, ns = not significant.

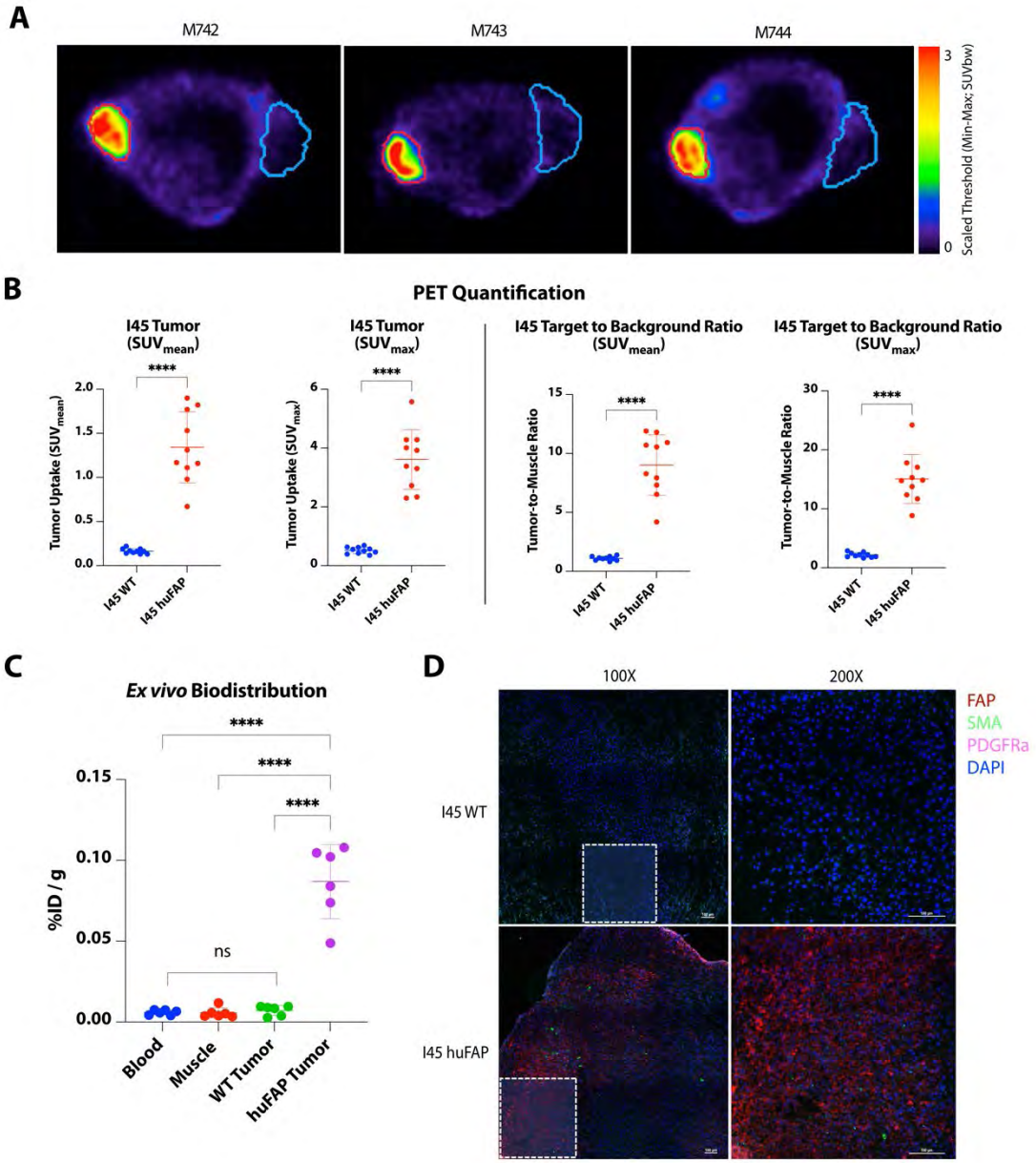

Figure 2. Imaging of FAP Expression in a I45 Mesothelioma Xenograft Model *In Vivo*

(A) Representative [^{18}F]AlF-FAPI-74 PET images of 3 different NSG mice (M742, M743, M744 refer to mouse number) xenografted with I45 WT (left side, blue ROI) and I45 huFAP mesothelioma tumor (right side, red ROI) showed a selective uptake of the tracer in the FAP-expressing, I45 huFAP tumor. [^{18}F]AlF-FAPI-74 PET/CT images were acquired 1 hour post-radiotracer administration. **(B)** For [^{18}F]AlF-FAPI-74 PET quantification, ROIs were drawn around I45 tumors and background muscle. The left panel shows the raw tumor uptake in SUV_{mean} and SUV_{max}, and the right panel shows the tumor-to-muscle ratio calculated by dividing the signal from the tumors by the signal from the muscle. I45 huFAP tumor demonstrated 7 to 8-fold higher tracer uptake relative to the WT tumor. n=10, data points are mean ± SD. Groups were compared using an unpaired t-test (two-tailed). ****p<0.0001. **(C)** *Ex vivo* biodistribution analysis performed following terminal [^{18}F]AlF-FAPI-74 imaging (approximately 1.5 hours post-radiotracer administration) showed 12 and 15-fold increased tracer retention in FAP-expressing huFAP tumor relative to the WT tumor and background organs, respectively. n=6, data points are mean ± SD. Groups were

compared using a one-way ANOVA with Tukey's multiple comparison test. ****p<0.0001, ns = not significant. **(D)** Representative IHC images of A549 tumor sections stained with antibodies against FAP, α-SMA, PDGFRα, and DAPI, demonstrate robust FAP expression in the I45 huFAP tumor. Scale = 100μm.

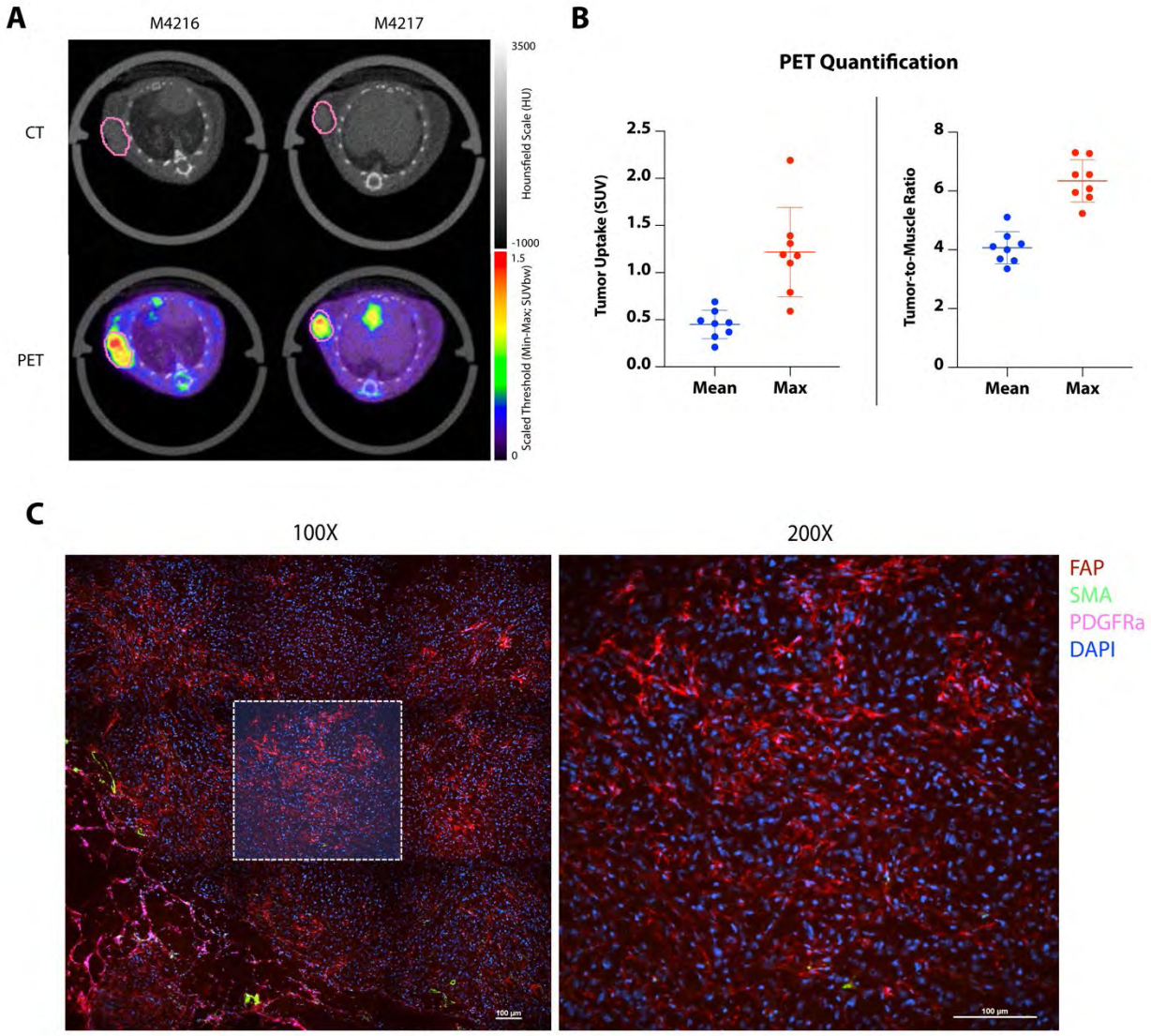

Figure 3. Imaging of Mouse Stromal FAP Expression in an A549 Lung Adenocarcinoma Xenograft Model *In Vivo*

(A) Representative [^{18}F]AlF-FAPI-74 PET images of 2 different NSG mice (M4216 and M4217 refer to mouse number) xenografted with A549 lung adenocarcinoma tumor (right side, pink ROI) 1 hour post-radiotracer administration demonstrated retention of [^{18}F]AlF-FAPI-74 tracer in the tumor area. **(B)** [^{18}F]AlF-FAPI-74 PET quantification, with the left panel showing the raw tumor uptake in SUV_{mean} and SUV_{max}, and the right panel shows the tumor-to-muscle ratio. Target-to-background ratio demonstrated 4 (SUV_{mean}) to 6.5-fold (SUV_{max}) higher uptake in the A549 tumor relative to muscle. n=8, data points are mean ± SD. **(C)** Representative IHC images of A549 tumor sections stained with antibodies against FAP, α-SMA, PDGFRα, and DAPI, demonstrate robust FAP expression in the tumor, validating PET imaging findings. Scale = 100µm.

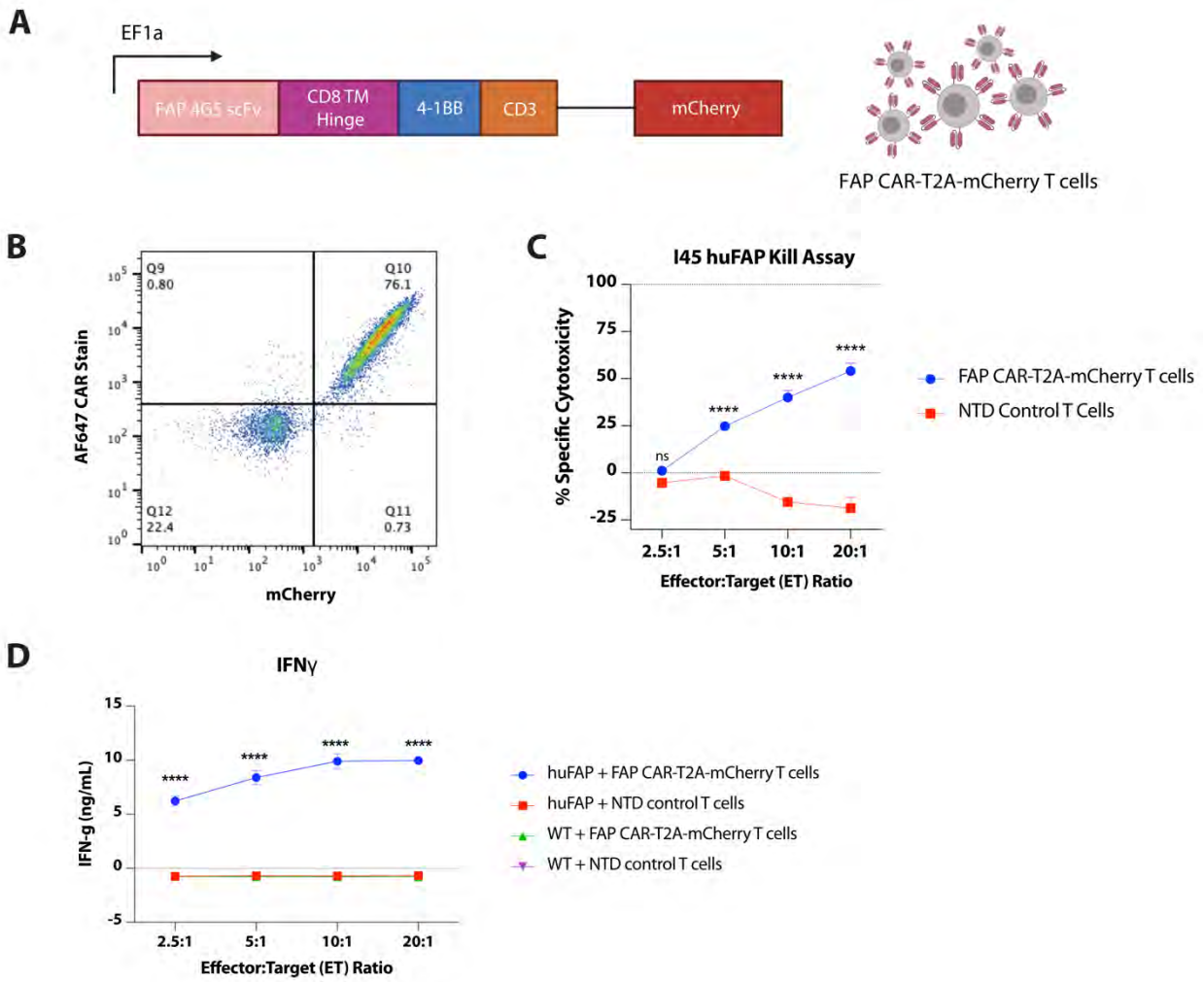

Figure 4: *In Vitro* Characterization and Validation of FAP CAR T Cell Effector Function

(A) Schematic of pTRPE L2HG FAP CAR-T2A-mCherry backbone. CD3 and mCherry are separated by a T2A cleavage site. **(B)** Primary human T cells were transduced with pTRPE L2HG FAP CAR-T2A-mCherry lentivirus at MOI of 5 and transduction efficiency was assessed with flow cytometry using mCherry and AF647-conjugated F(ab')$_2$ fragment. Transduced cells were sorted on mCherry expression and AF647 stain for downstream assays. **(C)** Target-specific cytolytic activity of FAP CAR T cells were tested by co-incubating them with I45 WT and I45 huFAP target cells overnight. The assay demonstrated an Effector-to-Target ratio (E:T)-dependent killing of the target cells. Percent specific cytotoxicity was determined using MTS assay. n=3, data points are mean ± SD. Groups were compared using a two-way ANOVA with Šídák's multiple comparisons test. ****p<0.0001, ns = not significant. **(D)** IFNγ and TNFα secretion from effector FAP CAR T cells following an overnight exposure to target I45 cells. The level of cytokine secretion was determined by ELISA. Data points are mean ± SD and groups were compared using a two-way ANOVA with Tukey's multiple comparisons test. ****p<0.0001.

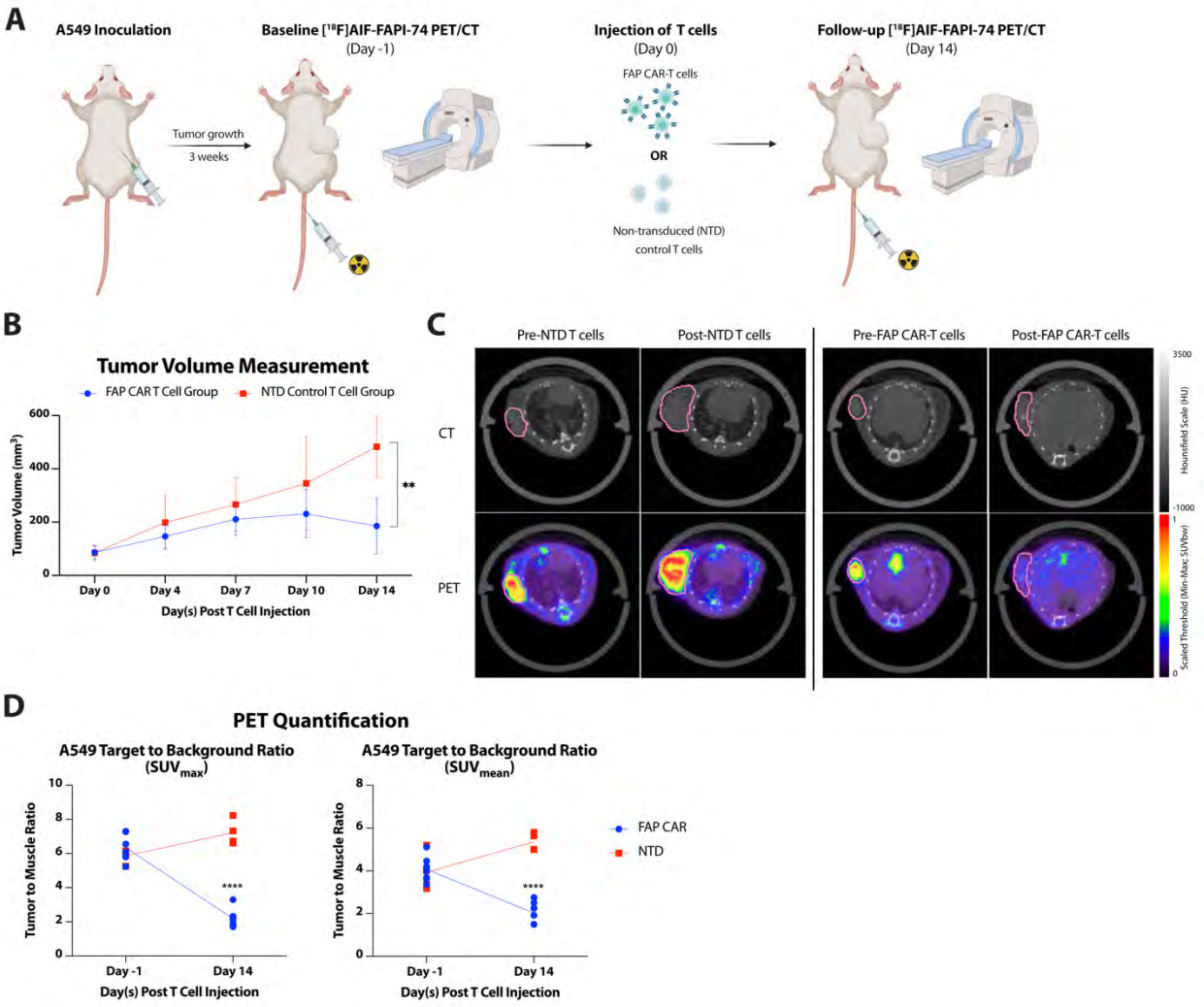

Figure 5: Monitoring of Therapeutic Response to FAP CAR T Cell Therapy

(A) Schematic of experimental timeline. NSG immunodeficient mice were subcutaneously xenografted with A549 tumor. The tumors were grown for 3 weeks, and all animals were imaged on small animal PET/CT 1 hour following [^{18}F]AlF-FAPI-74 administration to establish a baseline uptake. Animals were then randomized to receive either 5x10^{6} CAR^{+} FAP CAR T cells or cell number-matched non-transduced control (NTD) T cells via tail vein. The mice were imaged again with [^{18}F]AlF-FAPI-74 2 weeks following T cell injection for terminal PET imaging and downstream tissue processing. **(B)** Tumor volume data between CAR T cell injection (Day 0) and follow-up [^{18}F]AlF-FAPI-74 PET/CT scan (Day 14) demonstrated a statistically significant decrease in tumor volume for the FAP CAR T cell-treated group relative to the NTD control T cell-treated group. n=4 for NTD control T cell group, n=8 for FAP CAR T cell group. Data points are mean ± SD. Data for Day 14 between the two groups were compared using an unpaired t-test (two-tailed). **p=0.0011. **(C)** Representative [^{18}F]AlF-FAPI-74 PET/CT images showed statistical differences in tracer uptake between FAP CAR T cell-treated (right, M4917) and non-transduced (NTD) T cell-treated (left, M4916) animals. **(D)** [^{18}F]AlF-FAPI-74 PET quantification demonstrated a 2 (SUV_{mean}) to 3-fold (SUV_{max}) reduction in target tumor-to-muscle uptake ratio for FAP CAR T cell-treated group relative to the baseline scan. n=4 for NTD control T cell group, n=8 for FAP CAR T cell group. Data points are mean ± SD. Groups were compared using a one-way ANOVA with Tukey's multiple comparison test. *p=0.0151, ****p<0.0001.

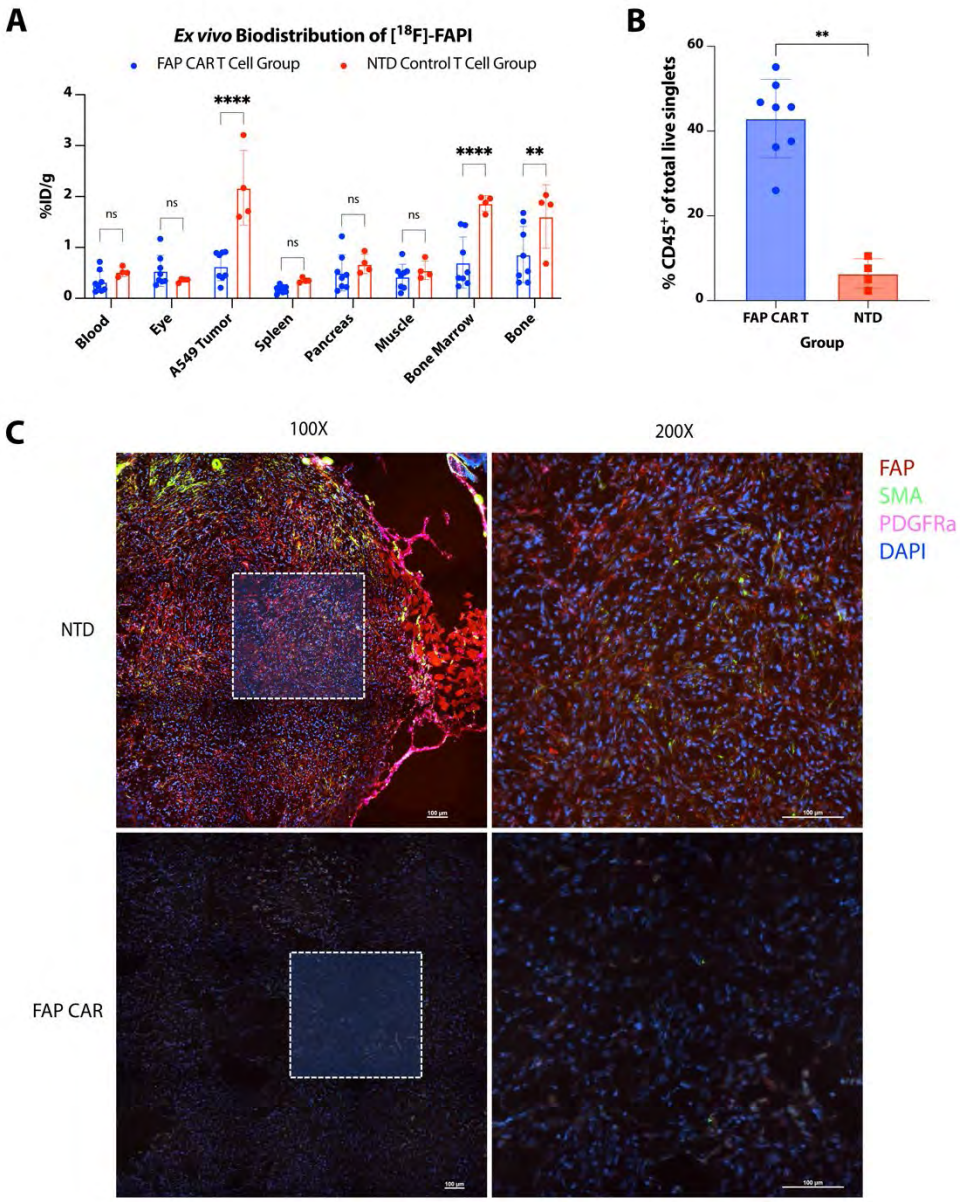

Figure 6: Tumor Measurement, *Ex Vivo* Biodistribution, and Tumor Analysis for Correlation with Radiologic Findings

(A) *Ex vivo* biodistribution analysis following the terminal [^{18}F]AlF-FAPI-74 PET/CT imaging time point on Day 14 showed around 3-fold higher tracer retention in the NTD control T cell-treated tumor compared to the FAP CAR T cell-treated tumor. Data points are mean ± SD and groups were compared using a two-way ANOVA with Šídák's multiple comparisons test. **p=0.0065, ****p<0.0001, ns = not significant. **(B)** Flow analysis of cell population in the A549 tumor treated with FAP CAR T cell vs. NTD control T cells showed a higher percentage of total CD45$^+$ in FAP CAR T cell-treated tumor. Groups were compared using a Mann-Whitney test. **p=0.0040. **(C)** Representative IHC images of A549 tumor sections stained with antibodies against FAP, α-SMA, PDGFRα, and DAPI. A549 tumor harvested from animals treated with FAP CAR T cells showed lack of FAP expression and patchy areas of apoptotic cells, whereas tumor harvested from NTD-treated animals showed intact and robust expression of FAP, validating PET imaging findings. Scale = 100μm.

627 **References**
628

629 1. Boyiadzis MM, Dhodapkar MV, Brentjens RJ, Kochenderfer JN, Neelapu SS, Maus MV*, et al.*
630 Chimeric antigen receptor (CAR) T therapies for the treatment of hematologic malignancies:
631 clinical perspective and significance. *J Immunother Cancer* 2018;**6**(1):137 doi 10.1186/s40425-
632 018-0460-5.
633 2. Watanabe K, Kuramitsu S, Posey AD, Jr., June CH. Expanding the Therapeutic Window for CAR T
634 Cell Therapy in Solid Tumors: The Knowns and Unknowns of CAR T Cell Biology. *Front Immunol*
635 2018;**9**:2486 doi 10.3389/fimmu.2018.02486.
636 3. Springuel L, Lonez C, Alexandre B, Van Cutsem E, Machiels JH, Van Den Eynde M*, et al.* Chimeric
637 Antigen Receptor-T Cells for Targeting Solid Tumors: Current Challenges and Existing Strategies.
638 *BioDrugs* 2019;**33**(5):515-37 doi 10.1007/s40259-019-00368-z.
639 4. Hinshaw DC, Shevde LA. The Tumor Microenvironment Innately Modulates Cancer Progression.
640 *Cancer Res* 2019;**79**(18):4557-66 doi 10.1158/0008-5472.CAN-18-3962.
641 5. Bejarano L, Jordao MJC, Joyce JA. Therapeutic Targeting of the Tumor Microenvironment. *Cancer*
642 *Discov* 2021;**11**(4):933-59 doi 10.1158/2159-8290.CD-20-1808.
643 6. Garin-Chesa P, Old LJ, Rettig WJ. Cell surface glycoprotein of reactive stromal fibroblasts as a
644 potential antibody target in human epithelial cancers. *Proceedings of the National Academy of*
645 *Sciences* 1990;**87**(18):7235-9.
646 7. Xing F, Saidou J, Watabe K. Cancer associated fibroblasts (CAFs) in tumor microenvironment. *Front*
647 *Biosci (Landmark Ed)* 2010;**15**(1):166-79 doi 10.2741/3613.
648 8. Xin L, Gao J, Zheng Z, Chen Y, Lv S, Zhao Z*, et al.* Fibroblast Activation Protein-alpha as a Target in
649 the Bench-to-Bedside Diagnosis and Treatment of Tumors: A Narrative Review. *Front Oncol*
650 2021;**11**:648187 doi 10.3389/fonc.2021.648187.
651 9. Duperret EK, Trautz A, Ammons D, Perales-Puchalt A, Wise MC, Yan J*, et al.* Alteration of the tumor
652 stroma using a consensus DNA vaccine targeting fibroblast activation protein (FAP) synergizes
653 with antitumor vaccine therapy in mice. *Clinical Cancer Research* 2018;**24**(5):1190-201.
654 10. Bughda R, Dimou P, D'Souza RR, Klampatsa A. Fibroblast Activation Protein (FAP)-Targeted CAR-T
655 Cells: Launching an Attack on Tumor Stroma. *Immunotargets Ther* 2021;**10**:313-23 doi
656 10.2147/ITT.S291767.
657 11. Kratochwil C, Flechsig P, Lindner T, Abderrahim L, Altmann A, Mier W*, et al.* (68)Ga-FAPI PET/CT:
658 Tracer Uptake in 28 Different Kinds of Cancer. *J Nucl Med* 2019;**60**(6):801-5 doi
659 10.2967/jnumed.119.227967.
660 12. Kakarla S, Chow KK, Mata M, Shaffer DR, Song X-T, Wu M-F*, et al.* Antitumor effects of chimeric
661 receptor engineered human T cells directed to tumor stroma. *Molecular Therapy*
662 2013;**21**(8):1611-20.
663 13. Lo A, Wang LS, Scholler J, Monslow J, Avery D, Newick K*, et al.* Tumor-Promoting Desmoplasia Is
664 Disrupted by Depleting FAP-Expressing Stromal Cells. *Cancer Res* 2015;**75**(14):2800-10 doi
665 10.1158/0008-5472.CAN-14-3041.
666 14. Schuberth PC, Hagedorn C, Jensen SM, Gulati P, van den Broek M, Mischo A*, et al.* Treatment of
667 malignant pleural mesothelioma by fibroblast activation protein-specific re-directed T cells. *J*
668 *Transl Med* 2013;**11**:187 doi 10.1186/1479-5876-11-187.
669 15. Giesel FL, Adeberg S, Syed M, Lindner T, Jimenez-Franco LD, Mavriopoulou E*, et al.* FAPI-74 PET/CT
670 Using Either (18)F-AlF or Cold-Kit (68)Ga Labeling: Biodistribution, Radiation Dosimetry, and
671 Tumor Delineation in Lung Cancer Patients. *J Nucl Med* 2021;**62**(2):201-7 doi
672 10.2967/jnumed.120.245084.

16. Ellebrecht CT, Bhoj VG, Nace A, Choi EJ, Mao X, Cho MJ*, et al.* Reengineering chimeric antigen receptor T cells for targeted therapy of autoimmune disease. *Science* 2016;**353**(6295):179-84 doi 10.1126/science.aaf6756.
17. Barrett RL, Pure E. Cancer-associated fibroblasts and their influence on tumor immunity and immunotherapy. *Elife* 2020;**9** doi 10.7554/eLife.57243.
18. Sellmyer MA, Lee IK, Mankoff DA. Building the Bridge: Molecular Imaging Biomarkers for 21(st) Century Cancer Therapies. *J Nucl Med* 2021 doi 10.2967/jnumed.121.262484.
19. Bensch F, van der Veen EL, Lub-de Hooge MN, Jorritsma-Smit A, Boellaard R, Kok IC*, et al.* (89)Zr-atezolizumab imaging as a non-invasive approach to assess clinical response to PD-L1 blockade in cancer. *Nat Med* 2018;**24**(12):1852-8 doi 10.1038/s41591-018-0255-8.
20. Makvandi M, Pantel A, Schwartz L, Schubert E, Xu K, Hsieh CJ*, et al.* A PET imaging agent for evaluating PARP-1 expression in ovarian cancer. *J Clin Invest* 2018;**128**(5):2116-26 doi 10.1172/JCI97992.
21. Fabre M, Ferrer C, Dominguez-Hormaetxe S, Bockorny B, Murias L, Seifert O*, et al.* OMTX705, a Novel FAP-Targeting ADC Demonstrates Activity in Chemotherapy and Pembrolizumab-Resistant Solid Tumor Models. *Clin Cancer Res* 2020;**26**(13):3420-30 doi 10.1158/1078-0432.CCR-19-2238.
22. Fu K, Pang Y, Zhao L, Lin L, Wu H, Sun L*, et al.* FAP-targeted radionuclide therapy with [(177)Lu]Lu-FAPI-46 in metastatic nasopharyngeal carcinoma. *Eur J Nucl Med Mol Imaging* 2021 doi 10.1007/s00259-021-05634-3.
23. Tanswell P, Garin-Chesa P, Rettig WJ, Welt S, Divgi CR, Casper ES*, et al.* Population pharmacokinetics of antifibroblast activation protein monoclonal antibody F19 in cancer patients. *Br J Clin Pharmacol* 2001;**51**(2):177-80 doi 10.1111/j.1365-2125.2001.01335.x.
24. Laverman P, van der Geest T, Terry SY, Gerrits D, Walgreen B, Helsen MM*, et al.* Immuno-PET and Immuno-SPECT of Rheumatoid Arthritis with Radiolabeled Anti-Fibroblast Activation Protein Antibody Correlates with Severity of Arthritis. *J Nucl Med* 2015;**56**(5):778-83 doi 10.2967/jnumed.114.152959.
25. Meletta R, Muller Herde A, Chiotellis A, Isa M, Rancic Z, Borel N*, et al.* Evaluation of the radiolabeled boronic acid-based FAP inhibitor MIP-1232 for atherosclerotic plaque imaging. *Molecules* 2015;**20**(2):2081-99 doi 10.3390/molecules20022081.
26. Altmann A, Haberkorn U, Siveke J. The Latest Developments in Imaging of Fibroblast Activation Protein. *J Nucl Med* 2021;**62**(2):160-7 doi 10.2967/jnumed.120.244806.
27. Siebermair J, Kessler L, Kupusovic J, Rassaf T, Rischpler C. Cardiac fibroblast activation detected by (68)Gallium-FAPI-46 positron emission tomography-magnetic resonance imaging as a sign of chronic activity in cardiac sarcoidosis. *Eur Heart J Case Rep* 2022;**6**(1):ytac005 doi 10.1093/ehjcr/ytac005.
28. Luo Y, Pan Q, Yang H, Peng L, Zhang W, Li F. Fibroblast Activation Protein-Targeted PET/CT with (68)Ga-FAPI for Imaging IgG4-Related Disease: Comparison to (18)F-FDG PET/CT. *J Nucl Med* 2021;**62**(2):266-71 doi 10.2967/jnumed.120.244723.
29. Notohamiprodjo S, Nekolla SG, Robu S, Villagran Asiares A, Kupatt C, Ibrahim T*, et al.* Imaging of cardiac fibroblast activation in a patient after acute myocardial infarction using (68)Ga-FAPI-04. *J Nucl Cardiol* 2021 doi 10.1007/s12350-021-02603-z.
30. Fletcher JW, Djulbegovic B, Soares HP, Siegel BA, Lowe VJ, Lyman GH*, et al.* Recommendations on the use of 18F-FDG PET in oncology. *Journal of Nuclear Medicine* 2008;**49**(3):480-508.
31. Bae S, Park CW, Son HK, Ju HK, Paik D, Jeon CJ*, et al.* Fibroblast activation protein alpha identifies mesenchymal stromal cells from human bone marrow. *Br J Haematol* 2008;**142**(5):827-30 doi 10.1111/j.1365-2141.2008.07241.x.

32. Roberts EW, Deonarine A, Jones JO, Denton AE, Feig C, Lyons SK*, et al.* Depletion of stromal cells expressing fibroblast activation protein-alpha from skeletal muscle and bone marrow results in cachexia and anemia. *J Exp Med* 2013;**210**(6):1137-51 doi 10.1084/jem.20122344.
33. Tran E, Chinnasamy D, Yu Z, Morgan RA, Lee CC, Restifo NP*, et al.* Immune targeting of fibroblast activation protein triggers recognition of multipotent bone marrow stromal cells and cachexia. *J Exp Med* 2013;**210**(6):1125-35 doi 10.1084/jem.20130110.
34. Rousset O, Rahmim A, Alavi A, Zaidi H. Partial Volume Correction Strategies in PET. *PET Clin* 2007;**2**(2):235-49 doi 10.1016/j.cpet.2007.10.005.
35. Soret M, Bacharach SL, Buvat I. Partial-volume effect in PET tumor imaging. *J Nucl Med* 2007;**48**(6):932-45 doi 10.2967/jnumed.106.035774.
36. Gulati P, Ruhl J, Kannan A, Pircher M, Schuberth P, Nytko KJ*, et al.* Aberrant Lck Signal via CD28 Costimulation Augments Antigen-Specific Functionality and Tumor Control by Redirected T Cells with PD-1 Blockade in Humanized Mice. *Clin Cancer Res* 2018;**24**(16):3981-93 doi 10.1158/1078-0432.CCR-17-1788.
37. Murthy P, Ekeke CN, Russell KL, Butler SC, Wang Y, Luketich JD*, et al.* Making cold malignant pleural effusions hot: driving novel immunotherapies. *Oncoimmunology* 2019;**8**(4):e1554969 doi 10.1080/2162402X.2018.1554969.
38. Dendl K, Koerber SA, Kratochwil C, Cardinale J, Finck R, Dabir M*, et al.* FAP and FAPI-PET/CT in Malignant and Non-Malignant Diseases: A Perfect Symbiosis? *Cancers (Basel)* 2021;**13**(19) doi 10.3390/cancers13194946.
39. Rurik JG, Tombacz I, Yadegari A, Mendez Fernandez PO, Shewale SV, Li L*, et al.* CAR T cells produced in vivo to treat cardiac injury. *Science* 2022;**375**(6576):91-6 doi 10.1126/science.abm0594.
40. Rohrich M, Leitz D, Glatting FM, Wefers AK, Weinheimer O, Flechsig P*, et al.* Fibroblast Activation Protein-Specific PET/CT Imaging in Fibrotic Interstitial Lung Diseases and Lung Cancer: A Translational Exploratory Study. *J Nucl Med* 2022;**63**(1):127-33 doi 10.2967/jnumed.121.261925.
41. White ES, Thomas M, Stowasser S, Tetzlaff K. Challenges for Clinical Drug Development in Pulmonary Fibrosis. *Front Pharmacol* 2022;**13**:823085 doi 10.3389/fphar.2022.823085.
42. Lindner T, Loktev A, Giesel F, Kratochwil C, Altmann A, Haberkorn U. Targeting of activated fibroblasts for imaging and therapy. *EJNMMI Radiopharm Chem* 2019;**4**(1):16 doi 10.1186/s41181-019-0069-0.
43. Kersting D, Settelmeier S, Mavroeidi I-A, Herrmann K, Seifert R, Rischpler C. Shining Damaged Hearts: Immunotherapy-Related Cardiotoxicity in the Spotlight of Nuclear Cardiology. *International Journal of Molecular Sciences* 2022;**23**(7):3802.
44. Finke D, Heckmann MB, Herpel E, Katus HA, Haberkorn U, Leuschner F*, et al.* Early detection of checkpoint inhibitor-associated myocarditis using 68Ga-FAPI PET/CT. *Frontiers in cardiovascular medicine* 2021;**8**:54.
45. Totzeck M, Siebermair J, Rassaf T, Rischpler C. Cardiac fibroblast activation detected by positron emission tomography/computed tomography as a possible sign of cardiotoxicity. *European Heart Journal* 2020;**41**(9):1060-.